

# Quantum-to-classical transition enabled by quadrature-PT symmetry

Wencong Wang,<sup>1</sup> Yanhua Zhai,<sup>2</sup> Dongmei Liu,<sup>1\*</sup> Xiaoshun

Jiang,<sup>3†</sup> Saeid Vashahri Ghamsari,<sup>4</sup> and Jianming Wen<sup>4‡</sup>

<sup>1</sup>Guangdong Provincial Key Laboratory of Quantum Engineering and Quantum Materials,

School of Physics and Telecommunication Engineering,

South China Normal University, Guangzhou 510006, China

<sup>2</sup> Physics Department, Spelman College, Atlanta, Georgia 30314, USA

<sup>3</sup>National Laboratory of Solid State Microstructures,

College of Engineering and Applied Sciences, Nanjing University, Nanjing 210093, China

<sup>4</sup>Department of Physics, Kennesaw State University, Marietta, Georgia 30060, USA

Quantum Langevin noise makes experimental realization of genuine quantum-optical parity-time (PT) symmetry in a gain-loss-coupled open system elusive. Here, we challenge this puzzle by exploiting twin beams produced from a nonlinear parametric process, one undergoing phase-sensitive linear quantum amplification (PSA) and the other engaging balanced loss merely. Unlike all previous studies involving phase-insensitive amplification (PIA), our PSA-loss scheme allows one quadrature pair to experience PT symmetry, a unique quantum effect without any classical counterpart. Such symmetry showcases many radical noise behaviors beyond conventional quantum squeezing and inaccessible to any PIA-based platform. Importantly, it is the only non-Hermitian system hitherto that enables the emergence of non-Hermiticity-induced quantum-to-classical transition for the same quantum observable when crossing exceptional point. Utilizing this quadrature-PT structure, we have further studied its potential in quantum sensing by exploring the quantum Cramér-Rao bound or Fisher information. Besides, the proposed quadrature PT symmetry also sheds new light on protecting continuous-variable (CV) qubits from decoherence in lossy transmission, a long-standing conundrum for various CV-based quantum technologies.

*Introduction.*—In canonical quantum mechanics, the system Hamiltonian as a physical observable is required to be Hermitian to ensure the realness of associated eigenspectra. Yet, it has long been known that the Hermiticity is just a sufficient but not necessary condition for a Hamiltonian to have real eigenvalues. This radical change of view stems from the seminal work by Bender and Boettcher in 1998, where a large class of non-Hermitian quantum Hamiltonians enjoying the joint parity-time (PT) symmetry was discovered to possess entirely real eigenvalues below a phase-transition point or exceptional point (EP) [1]. However, it remains elusive to probe such a non-Hermitian but PT-symmetric quantum

Hamiltonian experimentally due to the lack of complex quantum potential in reality. Nevertheless, the notion of PT symmetry [2-9] has successfully survived in many other physical branches. Thanks to the mathematical equivalence between the quantum Schrödinger and paraxial light propagation equation, classical optics was first suggested to simulate the wave properties of PT-symmetric quantum mechanics in synthesized settings. By incorporating linear gain and loss, optics has become a fertile ground for exploring PT symmetry [2-17] with an iconic feature of pair of eigenvalues phase transitioning from purely real to complex conjugate when a parameter crosses the EP. In this regard, a plethora of intriguing

phenomena have been uncovered by utilizing various linear and nonlinear optical materials to control and engineer light for practical applications [2-17].

Despite the impressive progress, to date the PT studies have been mostly limited to a mean-field approach that encapsulates all quantum dissipation in an ‘effective Hamiltonian’ [2-17]. This method treats light essentially as a (semi) classical electromagnetic (EM) field and only retains the minimum number of degrees of freedom to describe an open system. As a result, it fails to yield valid results when the nonclassicality of light are of interest. Notably, if the EM field is quantized, one must introduce the Langevin noise operator to preserve its corresponding commutation relation [18], though the introduction of quantum Langevin noise is generally thought to prevent the system from approaching quantum optical PT symmetry [19]. This is especially true when a phase-insensitive linear quantum amplifier (PIA) serves as an optical gain resource. Unfortunately, so far the research on PT optics has all been confined to PIA-based systems, thereby rendering the observation of quantum signatures highly challenging. The gain involvement also encounters another fundamental issue from the famous quantum noncloning theorem [20], namely how to maintain the integrity of the signal state, let alone the limitation further dictated by the Kramers-Kronig relation [21]. Therefore, it becomes a legitimate question whether gain-loss-coupled PT symmetry is viable quantum optically [19]. We notice that two alternative means have recently been implemented by using either a passive scheme or a non-Hermitian subset Hamiltonian in a large Hermitian system [22-27] to bypass the noise issues. These efforts have unearthed some quantum features, but they are incapable of providing a conclusive picture to the problem. We are also aware that a distinct trajectory is devoted to exploiting anti-PT symmetry [28-34], a counterpart of PT, to avoid the adverse effect of Langevin noise [35].

By overcoming the aforementioned obstacles, here we propose a novel and experimentally feasible platform utilizing twin beams generated from a nonlinear optical parametric process such as parametric down conversion (PDC) and four-wave mixing (FWM) [36], with the signal

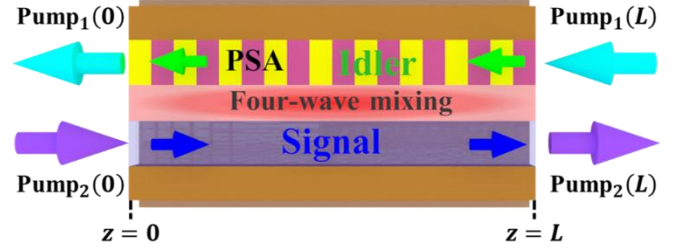


Fig. 1. PT symmetry undergone by twin beams from a backward-FWM process, where the  $-z$  idler mode experiences PSA and the  $+z$  signal faces equal loss.

arm experiencing pure loss while the idler channel undergoing phase-sensitive linear quantum amplification (PSA). Thanks to PSA-empowered noiseless amplification [37], our architecture not only makes the observation of true quantum optical PT a reality, but also displays distinctive features unapproachable to any previous scheme. Opposite to PIA equally amplifying paired quadratures with additive noise, PSA maximally amplifies some of them but inversely attenuates the rest without adding extra noise. This asymmetric amplification naturally gives rise to the so-called quadrature PT symmetry, a unique quantum effect without any classical counterpart. Given various never-before-seen attributes, our design further opens a door to uncovering the stunning classical-to-quantum transition for the same physical observable when a non-Hermitian parameter passes through the EP.

*Theoretical model.*—For simplicity, let us focus on the quadrature-PT setup schematic in Fig. 1, where under perfect phase matching, nondegenerate paired signal-idler waves are parametrically created from vacuum in a counterpropagating geometry by driving an FWM medium of length  $L$ . During their propagation, the idler and signal channels are respectively subject to PSA and loss with the rates of  $g$  and  $\gamma$ . For nondepleted and classical input pump lasers, the system evolves along the  $\mp z$  direction under the influence of the non-Hermitian Hamiltonian

$$H = \frac{i\hbar g(a_i^2 - a_i^{\dagger 2})}{2} - i\hbar \gamma a_s^\dagger a_s + \hbar \kappa (a_i^\dagger a_s^\dagger + a_i a_s), \quad (1)$$

and the signal-idler field operators  $(a_s, a_i)$  obey the Heisenberg-Langevin equations,

$$\frac{da_i}{dz} = ga_i^\dagger + ika_s^\dagger, \frac{da_s}{dz} = -\gamma a_s - ika_i^\dagger + f_s, \quad (2)$$

with  $\dagger$  denoting Hermitian conjugate,  $\kappa$  the parametric conversion strength, and  $f_s$  the quantum Langevin noise of zero mean satisfying  $\langle f_s(z)f_s^\dagger(z') \rangle = 2\gamma\delta(z-z')$  and  $\langle f_s^\dagger(z)f_s(z') \rangle = 0$ . At first glance, the dynamics (2) seems PT-irrelevant even if  $g = \gamma$ . Surprisingly, the hidden PT arises if one transforms Eq. (2) into the corresponding quadrature-operator evolution by defining  $q_j = (a_j^\dagger + a_j)/2$  and  $p_j = i(a_j^\dagger - a_j)/2$  ( $j = i, s$ ) with  $[q_j, p_j] = i/2$ . That is

$$\frac{d}{dz} \begin{bmatrix} q_i \\ p_s \end{bmatrix} = \begin{bmatrix} g & \kappa \\ -\kappa & -\gamma \end{bmatrix} \begin{bmatrix} q_i \\ p_s \end{bmatrix} + \begin{bmatrix} 0 \\ P_s \end{bmatrix}, \quad (3a)$$

$$\frac{d}{dz} \begin{bmatrix} p_i \\ q_s \end{bmatrix} = \begin{bmatrix} -g & \kappa \\ -\kappa & -\gamma \end{bmatrix} \begin{bmatrix} p_i \\ q_s \end{bmatrix} + \begin{bmatrix} 0 \\ Q_s \end{bmatrix}, \quad (3b)$$

where  $P_s = i(f_s^\dagger - f_s)/2$  and  $Q_s = (f_s^\dagger + f_s)/2$  are the Langevin-noise quadrature operators. The underlying physics now becomes apparent. The  $g$ - $\gamma$  introduction fundamentally intervenes the evolution of the usual two-mode squeezing. Specifically, for  $g = \gamma$ , albeit the impact of  $P_s$ ,  $\{q_i, p_s\}$  in Eq. (3a) become a PT-quadrature pair and adhere to PT-manifested noise reduction with the advent of nontrivial phase transition at the EP ( $\gamma = \kappa$ ) for the pair of eigen-propagation constants ( $\beta = \sqrt{\kappa^2 - \gamma^2}, -\beta$ ) transiting from purely real to conjugate imaginary. In contrast, the conjugate pair  $\{p_i, q_s\}$  in Eq. (3b) simply follow  $Q_s$ -mediated two-mode quadrature squeezing, with their propagation decoupled from  $\{q_i, p_s\}$ . Such asymmetric and contrasting dynamics are unavailable to any existing setting. More strikingly, the system will facilitate dual opposing quadrature PT symmetry— $\{q_i, p_s\}$  for active while  $\{p_i, q_s\}$  for passive, if without  $f_s$  and  $\gamma$ . The general solutions to Eqs. (3a) and (3b) are

$$\begin{bmatrix} q_i(0) \\ p_s(L) \end{bmatrix} = \sec(\beta L - \epsilon) \begin{bmatrix} \cos \epsilon & -\sin(\beta L) \\ -\sin(\beta L) & \cos \epsilon \end{bmatrix} \begin{bmatrix} q_i(L) \\ p_s(0) \end{bmatrix} + \sec(\beta L - \epsilon) \int_0^L dz P_s(z) \begin{bmatrix} -\sin(\beta(L-z)) \\ \cos(\beta z - \epsilon) \end{bmatrix}, \quad (4a)$$

$$\begin{bmatrix} p_i(0) \\ q_s(L) \end{bmatrix} = \sec(\kappa L) \begin{bmatrix} e^{\gamma L} & -\sin(\kappa L) \\ -\sin(\kappa L) & e^{-\gamma L} \end{bmatrix} \begin{bmatrix} p_i(L) \\ q_s(0) \end{bmatrix} + \sec(\kappa L) \int_0^L dz Q_s(z) \begin{bmatrix} -e^{\gamma z} \sin(\kappa(L-z)) \\ e^{\gamma(z-L)} \cos(\kappa z) \end{bmatrix}, \quad (4b)$$

with  $\epsilon = \arctan(\gamma/\beta)$ . From these solutions, indeed,

$\{q_i(0), p_s(L)\}$  but not  $\{p_i(0), q_s(L)\}$  carry on the PT-adjusted squeezing and anti-squeezing.

*Homodyne detection.*—To disclose quadrature PT symmetry, one straightforward way is to analyze the noise behaviors across the phase transition by homodyne detecting quadrature variances in comparison with the ideal squeezed vacuum. This in turn encourages us to look at the following four variances:  $\langle \Delta q_j^2 \rangle = \langle q_j^2 \rangle - \langle q_j \rangle^2$  and  $\langle \Delta p_j^2 \rangle = \langle p_j^2 \rangle - \langle p_j \rangle^2$ . Using Eqs. (4a) and (4b), after some lengthy algebra, one reaches

$$\langle \Delta q_{i,0}^2 \rangle = \frac{h(L) - 2\sin^2 \epsilon - \sec \epsilon \cos(2\beta L - \epsilon)}{8\cos^2(\beta L - \epsilon)}, \quad (5a)$$

$$\langle \Delta p_{s,L}^2 \rangle = \frac{h(L) \cos \epsilon - \cos(2\beta L + \epsilon) - 2\sin^2 \epsilon \cos(2\beta L - \epsilon)}{8\cos \epsilon \cos^2(\beta L - \epsilon)}, \quad (5b)$$

$$\langle \Delta q_{s,L}^2 \rangle = \frac{2 + \cos^2 \varphi e^{-2\gamma L} - \cos \varphi \cos(2\kappa L + \varphi)}{8\cos^2(\kappa L)}, \quad (5c)$$

$$\langle \Delta p_{i,0}^2 \rangle = \frac{(2 + \cos^2 \varphi) e^{2\gamma L} - \cos \varphi \cos(2\kappa L - \varphi)}{8\cos^2(\kappa L)}, \quad (5d)$$

where  $h(L) = 3 + 2\gamma L$  and  $\varphi = \tan^{-1}(\gamma/\kappa)$ . As expected, the PT-inherited variances (5a) and (5b) differentiate themselves from the rest two (5c) and (5d). A hallmark of such is the appearance of the argument  $\beta L$  in  $\langle \Delta q_{i,0}^2 \rangle$  and  $\langle \Delta p_{s,L}^2 \rangle$ . To have an intuitive picture, we exemplify these variances in Figs. 2(a)–(d) for some typical  $\gamma/\kappa$ . From Figs. 2(a) and (b), we observe a few extraordinary traits absent from all past studies on non-Hermitian physics as well as quantum squeezing. First, in the PT-phase intact region ( $\gamma < \kappa$ ), different from the two-mode squeezed vacuum (TMSV) with an oscillation period of  $2\pi$ , both  $\log_4 \langle \Delta q_{i,0}^2 \rangle$  and  $\log_4 \langle \Delta p_{s,L}^2 \rangle$  generally display increased classical fluctuations with a period  $T \approx 2\pi\kappa/\beta$ , except that the former shows a little sub-vacuum-noise suppression at a very short distance range due to the insufficient competition between PT and squeezing. In contrast, both cease to oscillate in the phase broken regime ( $\gamma > \kappa$ ) and are upper bounded by their respective variance curves at the EP. Moreover,  $\log_4 \langle \Delta p_{s,L}^2 \rangle$  always grows monotonically above the vacuum-noise level; while  $\log_4 \langle \Delta q_{i,0}^2 \rangle$  invariably exhibits quantum squeezing, and the larger  $\gamma/\kappa$  the larger the squeezing and  $L$ . What's more, the completely incompatible nature, quantum versus classical, of the

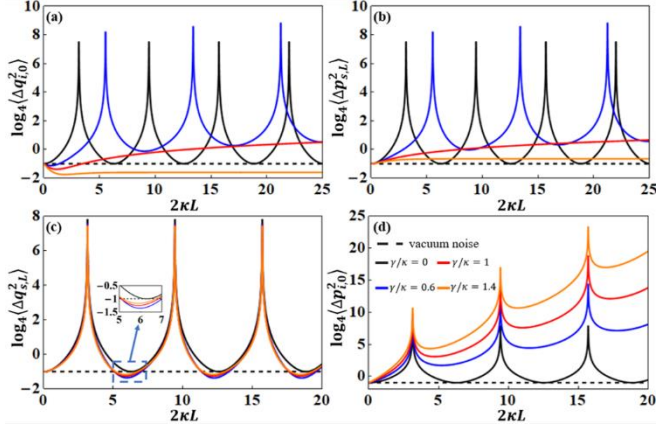


Fig. 2. PT-manifested  $\log_4\langle\Delta q_{i,0}^2\rangle$  (a) and  $\log_4\langle\Delta p_{s,L}^2\rangle$  (b) in the presence of quantum Langevin noise. Non-PT-symmetric but loss-noise-mediated  $\log_4\langle\Delta q_{s,L}^2\rangle$  (c) and  $\log_4\langle\Delta p_{i,0}^2\rangle$  (d). As the references, the black solid and dashed lines represent the regular TMSV ( $\gamma/\kappa = 0$ ) and vacuum noise, respectively.

same physical observable  $q_i(0)$  before and after the PT phase transition renders our system a unique candidate to study the transition between these two different worlds, whose boundary is physically defined by the EP curve. Contrarily, since  $\{p_i(0), q_s(L)\}$  are decoupled from  $\{q_i(0), p_s(L)\}$ , their variances fluctuate periodically, akin to the TMSV case. As shown in Figs. 2(c) and (d), though notably affected by  $Q_s$  and  $\gamma$ ,  $\log_4\langle\Delta q_{s,L}^2\rangle$  resembles the regular quadrature squeezing, but not  $\log_4\langle\Delta p_{i,0}^2\rangle$ .

From the above analysis, we learned that for the same single-mode quadrature, PT results in a nontrivial fundamental transition from quantum to classical when the non-Hermitian parameter  $\gamma$  oversteps a threshold. One may wonder whether this exotic phenomenon can also take place in a two-mode quadrature measurement. The answer is affirmative. To see how this works, we pay attention to  $d_1 = [q_i(0) + q_s(L)]/\sqrt{2}$  and  $d_2 = [p_i(0) + p_s(L)]/\sqrt{2}$ , which satisfy  $[d_1, d_2] = i/2$ . For the vacuum input, it is easy to check that their variances are simply the sum of the single-mode ones (5a)–(5d),

$$\langle\Delta d_1^2\rangle = \frac{\langle\Delta q_{i,0}^2\rangle + \langle\Delta q_{s,L}^2\rangle}{2}, \quad \langle\Delta d_2^2\rangle = \frac{\langle\Delta p_{i,0}^2\rangle + \langle\Delta p_{s,L}^2\rangle}{2}. \quad (6)$$

Based on Figs. 2(b) and (d),  $\langle\Delta d_2^2\rangle$  is expected to be distributed above the vacuum noise all the time.

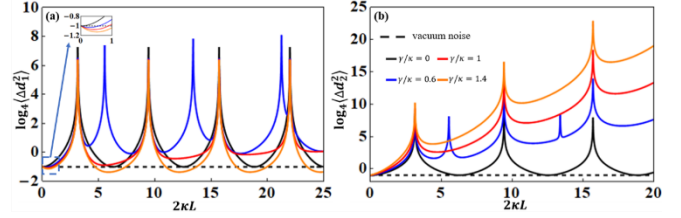


Fig. 3. PT-symmetric  $\log_4\langle\Delta d_1^2\rangle$  (a) and  $\log_4\langle\Delta d_2^2\rangle$  (b) with account of quantum noise. Again, as the references, the black solid and dashed curves are respectively the ideal TMSV ( $\gamma/\kappa = 0$ ) and vacuum noise.

Moreover, because  $\langle\Delta p_{s,L}^2\rangle$  and  $\langle\Delta p_{i,0}^2\rangle$  have different fluctuation periods before the phase transition, we envision that  $\langle\Delta d_2^2\rangle$  will exhibit interleaved dual periodic oscillations but reduce to a single period after the phase breaking. Though the situation becomes somewhat subtle for  $\langle\Delta d_1^2\rangle$ , its layout can be deduced similarly by compromising Figs. 2(a) and (c). To be specific, in the PT-phase unbroken region, it is a double-cycle growth fluctuation staggered on top of the vacuum noise (except the very short distance case). When PT symmetry spontaneously breaks down, counterintuitively, the single-period oscillating  $\langle\Delta d_1^2\rangle$  will always return certain squeezing at some effective distances, and these distances will be extended for a bigger  $\gamma/\kappa$ . Same as  $q_i(0)$ ,  $d_1$  can serve as another physical probe to visualize the quantum-to-classical transition induced by quadrature PT symmetry, too, with the boundary defined by the EP curve. All these statements excellently agree with our numerical simulations given in Figs. 3(a) and (b).

**RISM.**—Other than homodyne detection, there is one additional means to explore quadrature PT, the so-called relative intensity squeezing measurement (RISM). Traditionally, this method enables the shot-noise of one beam to be measured and subtracted from the other so as to attain lower-noise differential measurement of a signal of interest. To this end, we begin with our own relative-intensity operator,  $N_{i,0} - N_{s,L} = a_i^\dagger(0)a_i(0) - a_s^\dagger(L)a_s(L)$ . The degree of squeezing is then characterized by the noise figure (NF), which is determined by the relative-intensity variance. Mathematically, it takes the form [38]

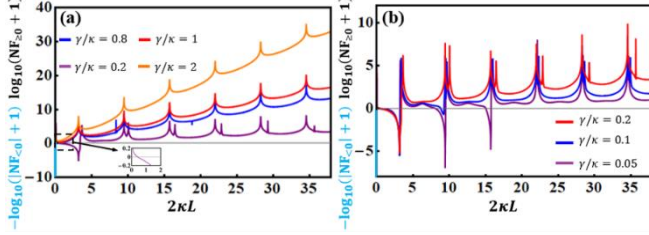


Fig. 4. (a) PT-regulated noise figure (NF) via relative intensity squeezing measurement. (b) Representative examples of quantum PT-symmetric NF.

$$\text{NF} = \frac{\text{Var}[N_{i,0} - N_{s,L}]}{\langle N_{i,0} \rangle + \langle N_{s,L} \rangle}. \quad (7)$$

Here, the average photon numbers are computed by plugging Eqs. (4a) and (4b) to  $\langle N_{i,0} \rangle = \langle q_i^2(0) \rangle + \langle p_i^2(0) \rangle - 1/2$  and  $\langle N_{s,L} \rangle = \langle q_s^2(L) \rangle + \langle p_s^2(L) \rangle - 1/2$ . In stark contrast to the quadrature variances discussed earlier, the NF, while bringing about some alike characteristics, clearly reveals some quite opposite peculiarities. For  $\gamma/\kappa \geq 1$ , as demonstrated in Fig. 4(a), in addition to the incremental single-period fluctuation  $\log_{10}(\text{NF}_{\geq 0} + 1)$  grows along with the increment of  $2\kappa L$ , and the larger  $\gamma/\kappa$  is, the noisier it is. From the plot, it is not difficult to conclude that in the PT-phase broken region, NF is essentially occupied by the noise anti-squeezing. However, NF behaves highly complex as  $\gamma/\kappa < 1$ . Although it is still an interleaved double-period oscillation within this range, the EP curve is no longer the partition to separate the classical and quantum fluctuations. In line with the numerical simulations, we find that quantum squeezing materializes when  $\gamma/\kappa < 0.52$ . Some representative examples are depicted in Fig. 4(b) by plotting  $-\log_{10}(\text{NF}_{< 0} + 1)$  for different  $\gamma/\kappa$ . Their comparison suggests that the smaller the value of  $\gamma/\kappa$ , the more pronounced the achievable squeezing over a longer distance  $2\kappa L$ . As a matter of fact, the RISM obviously supplies certain sharp signatures unreachable to the homodyne detection, regardless of the two highly unbalanced channels.

Before proceeding, a few remarks are ready here. First, even in the presence of Langevin noise, utilizing PSA instead of PIA is practicable to accomplish quantum optical PT under fair sampling measurement. Second,

contrary to PIA, PSA arouses the unusual quadrature PT and licenses the singular quantum-to-classical transition accompanied by the PT phase transition. Last but not least, quadrature PT sheds new light on protecting continuous-variable (CV) qubits from decoherence in inevitable lossy transmission, a long-standing conundrum for various CV-based quantum technologies [39].

*Quantum sensing.*—Being a discipline of practical application, quantum sensing [40–42] exploits quantum properties, effects, or systems to fulfill high-resolution and super-sensitive measurements of physical parameters over the similar measurements performed within a classical framework. For this, quantum squeezing has long been recognized as one of the indispensable nonclassical resources for ultra-precision estimations. Among them, one far-reaching example is its recent adoption by the Laser Interferometer Gravitational-Wave Observatory (LIGO) for gravitational wave detection. Nevertheless, the inevitable propagation loss often degrades the available squeezing and compromises the promised sensitivity. We note that in recent non-Hermitian studies, the abrupt change near EP has been capitalized for enhanced sensing in classical settings [43–47]. Yet, its extension to the quantum level turns out to be problematic because of quantum noise [48]. To avoid such noise, one usually resorts to either ideal anti-PT systems or post-selection measurement [25,34,35]. Unlike these studies, here we directly confront Langevin noise and explore the opportunity of quadrature PT in quantum sensing under fair sampling measurement. We are particularly interested to know whether the system could have any advantage in improving sensitivity. As shown below, the PT-quadrature observables can yield the best performance of classical sensing before the phase transition but departing far from the EP; while the non-PT-quadrature observables are capable of optimal quantum sensing by noise-mediated squeezing for  $\gamma/\kappa$  less than 1. This distinguishes our work from the previous anti-PT-, squeezing-, or EP-based proposals. Our analysis is carried out by estimating  $\kappa$  (or  $\gamma$ ) and comparing the achievable precision with the quantum Cramér-Rao bound (set by the quantum Fisher information of the

quantum state).

Suppose that the two bosonic modes are initially prepared in a coherent state  $|\psi_i\rangle = |\alpha_1, \alpha_2\rangle$ . An optimal homodyne measurement is then implemented on, say,  $q_i(0)$  after an evolution distance  $L$ . Using Eq. (4a), one can readily have its mean value and variance,

$$\langle q_i(0) \rangle = \frac{\cos \epsilon \langle q_i(L) \rangle - \sin(\beta L) \langle p_s(0) \rangle}{\cos(\beta L - \epsilon)}, \quad (8)$$

$$\langle \Delta q_{i,0}^2 \rangle = \frac{3 + w[2\gamma L - \tan \epsilon \sin(2\beta L)] - \cos(2\beta L) - 2\sin^2 \epsilon}{8\cos^2(\beta L - \epsilon)}, \quad (9)$$

where  $w = 2n_{th} + 1$  and  $n_{th}$  is the average thermal boson number. From Eqs. (8) and (9), it is clear that the Langevin noise shifts the peaks of  $\langle \Delta q_{i,0}^2 \rangle$  away from the troughs of  $\langle q_i(0) \rangle$ , so that they do not coincide at all. To ease the subsequent derivations, hereafter we assume  $\alpha_i = i\alpha_s^* = \sqrt{2}\alpha e^{i\pi/4}$ . The estimation precision relies on measuring the change of  $\langle q_i(0) \rangle$  due to a tiny perturbation  $\delta\kappa$  on a preset  $\kappa$ . This alternatively suggests to examine the system response to  $\langle q_i(0) \rangle$  for a small variation  $\delta\kappa$  around  $\kappa$ . We thus define the susceptibility to capture such a response,

$$\chi_\kappa^{q_i(0)} \equiv \frac{\partial \langle q_i(0) \rangle}{\partial \kappa} = \frac{\alpha\{2\beta L[\sin(\beta L) - 1] + \sin \epsilon[2\sin(\beta L) + \cos(\beta L - \epsilon) - \cos \epsilon]\}}{2\beta \cos^2(\beta L - \epsilon)}. \quad (10)$$

When  $\kappa \rightarrow \gamma$  or  $\beta \rightarrow 0$ ,  $\chi_\kappa^{q_i(0)} \rightarrow \alpha L(3 + \kappa^2 L^2)/[3(1 + \kappa L)^2]$  is a curvatureless constant, implying the loss of the sensing ability in the EP vicinity for the chosen observable. On the other hand, the  $\kappa$ -estimation is jointly determined by the variance and susceptibility,  $\Delta_{\kappa, q_{i,0}}^2 = \langle \Delta q_{i,0}^2 \rangle / [\chi_\kappa^{q_i(0)}]^2$ , whose inverse dictates the accuracy,

$$\Delta_{\kappa, q_{i,0}}^{-2} = \frac{2\alpha^2\{2\beta L[\sin(\beta L) - 1] + \sin \epsilon[2\sin(\beta L) + \cos(\beta L - \epsilon) - \cos \epsilon]\}^2}{\beta^2 \cos^2(\beta L - \epsilon)\{3 + w[2\gamma L - \tan \epsilon \sin(2\beta L)] - \cos(2\beta L) - 2\sin^2 \epsilon\}}. \quad (11)$$

The sensing fulfillment is to compare  $\Delta_{\kappa, q_{i,0}}^{-2}$  with the quantum Fisher information,  $F_\kappa$ , which sets the ultimate precision, i.e., the lower quantum Cramér-Rao bound for any optimal measurement,  $F_\kappa \geq \Delta_{\kappa, q_{i,0}}^{-2}$ .  $F_\kappa$  can be accordingly derived from

$$F_\kappa = 4L^2 (\langle \psi_f | \partial_\kappa H^\dagger \partial_\kappa H | \psi_f \rangle - \langle \psi_f | \partial_\kappa H^\dagger | \psi_f \rangle \langle \psi_f | \partial_\kappa H | \psi_f \rangle). \quad (12)$$

for the final state  $|\psi_f\rangle$  of the system in the Schrödinger

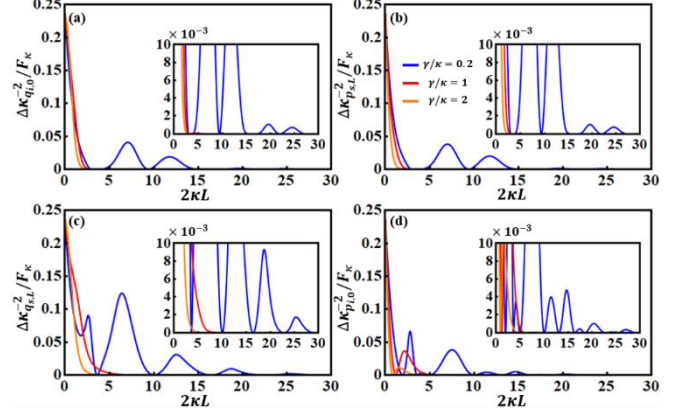


Fig. 5. Quantum sensing in quadrature PT symmetry characterized by the ratios of  $\Delta_{\kappa, q_{i,0}}^{-2}$  (a),  $\Delta_{\kappa, p_{s,L}}^{-2}$  (b),  $\Delta_{\kappa, q_{s,L}}^{-2}$  (c), and  $\Delta_{\kappa, p_{i,0}}^{-2}$  (d) to the quantum Fisher information  $F_\kappa$  for the parameters  $\{\alpha = 2, \gamma = 0.2, \kappa = 1\}$  (blue),  $\{2, 1, 1\}$  (red), and  $\{2, 2, 1\}$  (orange), respectively.

representation. As detailed in Supplementary Information, one can perform similar sensing evaluations to the rest three quadratures. Basing on the calculations shown in Figs. 5(a) and (b), we note that in the current arrangement,  $q_i(0)$  and  $p_s(L)$  can only permit optimal classical sensing for a moderate medium length in the phase-unbroken regime but away from the EP, as revealed by the ratios of  $\Delta_{\kappa, q_{i,0}}^{-2}/F_\kappa$  and  $\Delta_{\kappa, p_{s,L}}^{-2}/F_\kappa$ . On the contrary,  $q_s(L)$  and  $p_i(0)$  behave distinctively in the sense that, despite the impacts of the photon loss and Langevin noise, they are still able to offer optimal quantum sensing over a relatively longer distance for smaller  $\gamma/\kappa$ , as sketched in Figs. 5(c) and (d).

In short, fundamentally different from all previous research, the PSA-induced quadrature PT enables a unique way to observe a quantum-to-classical transition for a physical observable at the breakdown of symmetry. Such quadrature PT radically reshapes the dynamics of two-mode squeezing with a striking phase transition never seen before. Unfortunately, optical loss and Langevin noise hinder the PT quadrature pair to confer a quantum advantage in improving sensitivity, although the non-PT pair can still offer optimal quantum sensing. Besides of nonlinear wave mixing, our model can be also

achieved in other platforms such as superconducting circuits. Most importantly, our work forges a new avenue to explore the long-sought, nontrivial quantum-to-classical transition utilizing non-Hermitian physics.

**Acknowledgements.**—This work was supported by NSF 1806519 and NSF EFMA-1741693. X.J. acknowledges the support by the National Key R&D Program of China (2021YF A1400803). D.L. was supported by the Nature Science Foundation of Guangdong Province (2019A1515011401).

**AUTHOR CONTRIBUTIONS.**—J.W. conceived the theoretical scheme and supervised the whole project with the help of D.L. and X.J. W.W., supervised by J.W., carried out the whole calculations with the assistance of Y.Z. and S.V.G. All authors contributed to the discussions and writing of the manuscript.

\* [dmliu@scnu.edu.cn](mailto:dmliu@scnu.edu.cn)

† [jxs@nju.edu.cn](mailto:jxs@nju.edu.cn)

‡ [jianming.wen@kennesaw.edu](mailto:jianming.wen@kennesaw.edu)

- [1] Bender, C. M. & Boettcher, S. Real spectra in non-Hermitian Hamiltonians having PT symmetry. *Phys. Rev. Lett.* 80, 5243-5246 (1998).
- [2] El-Ganainy, R., Makris, K. G., Khajavikhan, M., Musslimani, Z. H., Rotter, S. & Christodoulides, D. N. Non-Hermitian physics and PT symmetry. *Nat. Phys.* 14, 11-19 (2018).
- [3] Özdemir, S. K., Rotter, S., Nori, F. & Yang, L. Parity-time symmetry and exceptional points in photonics. *Nat. Mater.* 18, 783-798 (2018).
- [4] Wen, J., Jiang, X., Jiang, L. & Xiao, M. Parity-time symmetry in optical microcavity systems. *J. Phys. B: At. Mol. Opt. Phys.* 51, 222001 (2018).
- [5] Feng, L., El-Ganainy, R. & Ge, L. Non-Hermitian photonics based on parity-time symmetry. *Nat. Photon.* 11, 752-762 (2017).
- [6] Konotop, V. V., Yang, J. & Zezyulin, D. A. Nonlinear waves in PT-symmetric systems. *Rev. Mod. Phys.* 88, 035002 (2016).
- [7] Miri, M.-A. & Alù, A. Exceptional points in optics and photonics. *Science* 363, eaar7709 (2019).
- [8] Longhi, S. Parity-time symmetry meets photonics: A new twist in non-Hermitian optics. *EPL* 120, 64001 (2018).
- [9] Zhang, Z., Ma, D., Sheng, J., Zhang, Y. & Xiao, M. Non-Hermitian optics in atomic systems. *J. Phys. B: At. Mol. Opt. Phys.* 51, 072001 (2018).
- [10] Rotter, C. E., Makris, K. G., El-Ganainy, R., Christodoulides, D. N., Segev, M. & Kip, D. Observation of parity-time symmetry in optics. *Nat. Phys.* 6, 192-195 (2010).
- [11] Guo, A., Salamo, G. J., Duchesne, D., Morandotti, R., Volatier-Ravat, M., Aimez, V., Siviloglou, G. A. & Christodoulides, D. N. Observation of PT-symmetry breaking in complex optical potentials. *Phys. Rev. Lett.* 103, 093902 (2009).
- [12] Regensburger, A., Bersch, C., Miri, M.-A., Onishchukov, G., Christodoulides, D. N. & Peschel, U. Parity-time synthetic photonic lattices. *Nature* 488, 167-171 (2012).
- [13] Chang, L., Jiang, X., Hua, S., Yang, C., Wen, J., Jiang, L., Li, G., Wang, G. & Xiao, M. Parity-time symmetry and variable optical isolation in active-passive-coupled microresonators. *Nature Photon.* 8, 524-529 (2014).
- [14] Peng, B., Özdemir, S. K., Lei, F., Monifi, F., Gianfreda, M., Long, G. L., Fan, S., Nori, F., Bender, C. M. & Yang, L. Parity-time-symmetric whispering-gallery microcavities. *Nat. Phys.* 10, 394-398 (2014).
- [15] Feng, L., Wong, Z. J., Ma, R.-M., Wang, Y. & Zhang, X. Single-mode laser by parity-time symmetry breaking. *Science* 346, 972-974 (2014).
- [16] Hodaei, H., Miri, M.-A., Heinrich, M., Christodoulides, D. N. & Khajavikhan, M. Parity-time-symmetric microring lasers. *Science* 346, 975-978 (2014).
- [17] Ma, J., Wen, J., Hu, Y., Ding, S., Jiang, X., Jiang, L. & Xiao, M. Chip-based optical isolator and nonreciprocal parity-time symmetry induced by stimulated Brillouin scattering. *Laser Photon. Rev.* 14, 1900278 (2020).
- [18] Agarwal, G. & Qu, K. Spontaneous generation of photons in transmission of quantum fields in PT-symmetric optical systems. *Phys. Rev. A* 85, 031802 (2012).
- [19] Scheel, S. & Szameit, A. PT-symmetric photonic quantum systems with gain and loss do not exist. *EPL* 122 34001 (2018).
- [20] Wootters, W. & Zurek, W. A single quantum cannot be cloned. *Nature* 299, 802-803 (1982).
- [21] Lee, Y.-C., Hsieh, M.-H., Flammia, S. T. & Lee, R.-K. Local PT symmetry violates the no-signaling principle. *Phys. Rev. Lett.* 112, 130404 (2014).
- [22] Klauck, F., Teuber, L., Ornigotti, M., Heinrich, M., Scheel, S. & Szameit, A. Observation of PT-

- symmetric quantum interference. *Nat. Photon.* 13, 883-887 (2019).
- [23] Naghiloo, M., Abbasi, M., Joglekar, Y. N. & Murch, K. W. Quantum state tomography across the exceptional point in a single dissipative qubit. *Nat. Phys.* 15, 1232-1236 (2019).
- [24] Wu, J., Liu, W., Geng, J., Song, X., Ye, X., Duan, C.-K., Rong, X. & Du, J. Observation of parity-time symmetry breaking in a single-spin system. *Science* 364, 878-880 (2019).
- [25] Li, Z. P., Yang, Y. Z., Chen, G., Han, Y. J., Li, C. F. & Guo, G. C. Experimental investigation of quantum PT-enhanced sensor. *Phys. Rev. Lett.* 125, 240506 (2020).
- [26] Ding, L., Shi, K., Zhang, Q., Shen, D., Zhang, X. & Zhang, W. Experimental determination of PT-symmetric exceptional points in a single trapped ion. *Phys. Rev. Lett.* 126, 083604 (2021).
- [27] Han, P.-R., Wu, F., Huang, X.-J., Wu, H., Yang, Z.-B., Zou, C.-L., Yi, W., Zhang, M., Li, H., Xu, K., Zheng, D., Fan, H., Wen, J. & Zheng, S.-B. PT symmetry and PT-enhanced quantum sensing in a spin-boson system. *arXiv:2210.04494* (2022).
- [28] Peng, P., Cao, W., Shen, C., Qu, W., Wen, J., Jiang, L. & Xiao, Y. Anti-parity-time symmetry in flying atoms. *Nat. Phys.* 12, 1139-1145 (2016).
- [29] Fan, H., Chen, J., Zhao, Z., Wen, J. & Huang, Y.-P. Anti-parity-time symmetry in passive nanophotonics. *ACS Photon.* 7, 3035-3041 (2020).
- [30] Li, Y., Peng, Y.-G., Han, L., Miri, M.-A., Li, W., Xiao, M., Zhu, X.-F., Zhao, J., Al' u, A., Fan, S. & Qiu, C.-W. Anti-parity-time symmetry in diffusive systems. *Science* 364, 170-173 (2019).
- [31] Jiang, Y., Mei, Y., Zuo, Y., Zhai, Y., Li, J., Wen, J. & Du, S. Anti-parity-time symmetric optical four-wave mixing in cold atoms. *Phys. Rev. Lett.* 123, 193604 (2019).
- [32] Zhang, X.-L., Jiang, T. & Chan, C. T. Dynamically encircling an exceptional point in anti-parity-time symmetric systems: asymmetric mode switching for symmetry-broken modes. *Light: Sci. Appl.* 8, 88 (2019).
- [33] Bergman, A., Duggan, R., Sharma, K., Tur, M., Zadok, A. & Al' u, A. Observation of anti-parity-time-symmetry, phase transitions and exceptional points in an optical fibre. *Nat. Commun.* 12, 486 (2021).
- [34] Wang, Y.-X. & Clerk, A. A. Non-Hermitian dynamics without dissipation in quantum systems. *Phys. Rev. A* 99, 063834 (2019).
- [35] Luo, X.-H., Zhang, C. & Du, S. Quantum squeezing and sensing with pseudo-anti-parity-time symmetry. *Phys. Rev. Lett.* 128, 173602 (2022).
- [36] Scully, M. O. & Zubairy, M. S. *Quantum Optics* (Cambridge, United Kingdom, 1997). B. Li, L. Wang, G. Casati, Thermal Diode: Rectification of Heat Flux. *Physical Review Letters* 93, 184301 (2004).
- [37] Loudon, R. Theory of noise accumulation in a linear optical-amplifier chains. *IEEE J. Quantum Electron.* QE-21, 766-773 (1985).
- [38] Japers, M., Turner, L. D. & Scholten, R. E. Relative intensity squeezing by four-wave mixing with loss: an analytic model and experimental diagnostic. *Opt. Express* 19, 3765-3774 (2011).
- [39] Braunstein, S. L. & van Loock, P. Quantum information with continuous variables. *Rev. Mod. Phys.* 77, 513-577 (2005).
- [40] Degen, C. L., Reinhard, F. & Cappellaro, P. Quantum sensing. *Rev. Mod. Phys.* 89, 035002 (2017).
- [41] Pezz' e, L., Smerzi, A., Oberthaler, M. K., Schmied, R. & Treutlein, P. Quantum metrology with nonclassical states of atomic ensembles. *Rev. Mod. Phys.* 90, 035005 (2018).
- [42] Giovannetti, V., Lloyd, S. & Maccone, L. Advances in quantum metrology. *Nat. Photon.* 5, 222-229 (2011).
- [43] Wiersig, J. Enhancing the sensitivity of frequency and energy splitting detection by using exceptional points: Application to microcavity sensors for single-particle detection. *Phys. Rev. Lett.* 112, 203901 (2014).
- [44] Wiersig, J. Review of exceptional point-based sensors. *Photon. Res.* 8, 1457-1467 (2020).
- [45] Liu, Z. P., Zhang, J., Özdemir, S. K., Peng, B., Jing, H., L' u, X. Y., Li, C. W., Yang, L., Nori, F. & Liu, Y. X. Metrology with PT-symmetric cavities: enhanced sensitivity near the PT-phase transition. *Phys. Rev. Lett.* 117, 110802 (2016).
- [46] Chen, W., Özdemir, S. K., Zhao, G., Wiersig, J. & Yang, L. Exceptional points enhance sensing in an optical microcavity. *Nature* 548, 192-196 (2017).
- [47] Hodaei, H., Hassan, A. U., Wittek, S., Garcia-Gracia, H., El-Ganainy, R., Christodoulides, D. N. & Khajavikhan, M. Enhanced sensitivity at higher-order exceptional points. *Nature* 548, 187-191 (2017).
- [48] Zhang, M., Sweeney, W., Hsu, C. W., Yang, L., Stone, A. D. & Jiang, L. Quantum noise theory of exceptional point amplifying sensors. *Phys. Rev. Lett.* 123, 180501 (2019).

# Supplementary Information for “Quantum-to-classical transition enabled by quadrature-PT symmetry”

Wencong Wang, Yanhua Zhai, Dongmei Liu\*, Xiaoshun Jiang\*,  
Saeid Vashahri Ghamsari, and Jianming Wen\*

Emails: [dmliu@scnu.edu.cn](mailto:dmliu@scnu.edu.cn); [jxs@nju.edu.cn](mailto:jxs@nju.edu.cn); [jianming.wen@kennesaw.edu](mailto:jianming.wen@kennesaw.edu)

## I. Derivation of the Heisenberg-Langevin equations

In our previous work [1], we have theoretically proved that a forward parametric optical process may lead to anti-PT symmetry while a backward parametric optical process can result in PT symmetry. For this reason, as schematic in Fig. 1 in the main text [2], we are interested in a backward nonlinear parametric optical process such as backward four-wave mixing, where the two counter-propagating parametric modes, idler and signal, respectively experience balanced phase-sensitive linear quantum amplification (PSA) and attenuation in their own channels within the medium of length  $L$ . For such an open system, the evolution of the paired idler and signal field operators is effectively determined by a non-Hermitian Hamiltonian,

$$H = i\frac{\hbar g}{2}(a_i^{\dagger 2} - a_i^2) - i\hbar\gamma a_s^{\dagger} a_s + \hbar\kappa(a_i^{\dagger} a_s^{\dagger} + a_i a_s), \quad (\text{S1.1})$$

where  $g$  and  $\gamma$  respectively denote the PSA rate and loss rate. From Eq. (S1.1), one can readily obtain the Heisenberg equations of the idler-signal field operators,

$$i\hbar \frac{\partial a_i}{\partial(-z)} = [a_i, H], \quad (\text{S1.2a})$$

$$i\hbar \frac{\partial a_s}{\partial z} = [a_s, H]. \quad (\text{S1.2b})$$

Thanks to the noiseless amplification empowered by the PSA, the idler dynamics is not subject to the additive noise and the commutation relation can be always satisfied throughout the whole process. However, this is not true for the lossy signal propagation. To restore the commutation relation, one has to introduce the quantum Langevin noise in the Heisenberg equation of the signal field operator. In this way, we arrive at the following coupled Heisenberg-Langevin equations for the system of interest,

$$\frac{\partial a_i}{\partial z} = g a_i^{\dagger} + i\kappa a_s^{\dagger}, \quad (\text{S1.3a})$$

$$\frac{\partial a_s}{\partial z} = -\gamma a_s - i\kappa a_i^{\dagger} + f_s. \quad (\text{S1.3b})$$

Though Eqs. (S1.3a) and (S1.3b) seem to have nothing to do with PT symmetry at first glance, as pointed out in the main text, the hidden PT symmetry arises if transforming both equations into the dynamics of the corresponding quadrature operators,  $q_j = (a_j^{\dagger} + a_j)/2$  and  $p_j = i(a_j^{\dagger} - a_j)/2$  ( $j = i, s$ ) with  $[q_j, p_j] = i/2$ . For simplicity, we concentrate on the case of the balanced PSA and loss,  $g = \gamma$ . With these preparations, one can easily attain the following sets of the coupled-quadrature equations

$$\frac{d}{dz} \begin{bmatrix} q_i \\ p_s \end{bmatrix} = \begin{bmatrix} \gamma & \kappa \\ -\kappa & -\gamma \end{bmatrix} \begin{bmatrix} q_i \\ p_s \end{bmatrix} + \begin{bmatrix} 0 \\ P_s \end{bmatrix}, \quad (\text{S1.4a})$$

$$\frac{d}{dz} \begin{bmatrix} p_i \\ q_s \end{bmatrix} = \begin{bmatrix} -\gamma & \kappa \\ -\kappa & -\gamma \end{bmatrix} \begin{bmatrix} p_i \\ q_s \end{bmatrix} + \begin{bmatrix} 0 \\ Q_s \end{bmatrix}, \quad (\text{S1.4b})$$

with  $P_s = i(f_s^{\dagger} - f_s)/2$  and  $Q_s = (f_s^{\dagger} + f_s)/2$  being the Langevin-noise quadrature operators. From Eq. (S1.4a), one can derive the effective Hamiltonian matrix for the quadrature pair  $(q_i, p_s)$ , which reads

$$H_{(q_i, p_s)} = \begin{bmatrix} i\gamma & i\kappa \\ -i\kappa & -i\gamma \end{bmatrix}. \quad (\text{S1.5})$$

It is straightforward to show that  $H_{(q_i, p_s)}$  is indeed PT-symmetric, because it satisfies  $PTH_{(q_i, p_s)} = H_{(q_i, p_s)}PT$  for the combined PT operation with the parity operator being  $P = \begin{bmatrix} 0 & 1 \\ 1 & 0 \end{bmatrix}$  and the time-reversal operator assuming the complex conjugation. For this reason, we call  $(q_i, p_s)$  the PT-

quadrature pair. This is in a sharp contrast to the effective Hamiltonian matrix  $H_{(p_i, q_s)} = \begin{bmatrix} -i\gamma & i\kappa \\ -i\kappa & -i\gamma \end{bmatrix}$  in Eq. (S1.4b) for the other conjugate quadrature pair  $(p_i, q_s)$ , which is apparently irrelevant to PT symmetry. The two eigenvalues of  $H_{(q_i, p_s)}$  are  $\beta_{\pm} = \pm\sqrt{\kappa^2 - \gamma^2}$ . Akin to the classical PT symmetry,  $\frac{\gamma}{\kappa} < 1$  corresponds to the quadrature PT-phase unbroken regime while for  $\frac{\gamma}{\kappa} > 1$ , quadrature PT symmetry spontaneously breaks down. The quadrature PT phase transition occurs at the singular or exceptional point (EP),  $\frac{\gamma}{\kappa} = 1$ . In terms of the initial boundary conditions, the general solutions of Eqs. (S1.4a) and (S1.4b) are readily found to be

$$\begin{bmatrix} q_i(0) \\ p_s(L) \end{bmatrix} = \sec(\beta L - \epsilon) \begin{bmatrix} \cos \epsilon & -\sin(\beta L) \\ -\sin(\beta L) & \cos \epsilon \end{bmatrix} \begin{bmatrix} q_i(L) \\ p_s(0) \end{bmatrix} + \sec(\beta L - \epsilon) \int_0^L dz P_s(z) \begin{bmatrix} -\sin(\beta(L-z)) \\ \cos(\beta z - \epsilon) \end{bmatrix}, \quad (\text{S1.6a})$$

$$\begin{bmatrix} p_i(0) \\ q_s(L) \end{bmatrix} = \sec(\kappa L) \begin{bmatrix} e^{\gamma L} & -\sin(\kappa L) \\ -\sin(\kappa L) & e^{-\gamma L} \end{bmatrix} \begin{bmatrix} p_i(L) \\ q_s(0) \end{bmatrix} + \sec(\kappa L) \int_0^L dz Q_s(z) \begin{bmatrix} -e^{\gamma z} \sin(\kappa(L-z)) \\ e^{\gamma(z-L)} \cos(\kappa z) \end{bmatrix}, \quad (\text{S1.6b})$$

with  $\epsilon = \arctan\left(\frac{\gamma}{\beta}\right)$ . It is not difficult to prove that the dynamical solutions (S1.6a) and (S1.6b) well maintain the commutation relations at all times,

$$\begin{aligned} [q_i(0), p_i(0)] &= \frac{e^{\gamma L} \cos \epsilon}{\cos(\beta L - \epsilon) \cos(\kappa L)} [q_i(L), p_i(L)] \\ &+ \frac{\sin(\beta L) \sin(\kappa L)}{\cos(\beta L - \epsilon) \cos(\kappa L)} [p_s(0), q_s(0)] \\ &+ \int_0^L dz \frac{e^{\gamma z} \sin(\beta(L-z)) \sin(\kappa(L-z))}{\cos(\beta L - \epsilon) \cos(\kappa L)} [P_s, Q_s] = \frac{i}{2}, \end{aligned} \quad (\text{S1.7a})$$

$$\begin{aligned} [q_s(L), p_s(L)] &= \frac{\sin(\beta L) \sin(\kappa L)}{\cos(\beta L - \epsilon) \cos(\kappa L)} [p_i(L), q_i(L)] \\ &+ \frac{e^{-\gamma L} \cos \epsilon}{\cos(\beta L - \epsilon) \cos(\kappa L)} [q_s(0), p_s(0)] \\ &+ \int_0^L dz \frac{e^{\gamma(z-L)} \cos(\beta z - \epsilon) \cos(\kappa z)}{\cos(\beta L - \epsilon) \cos(\kappa L)} [Q_s, P_s] = \frac{i}{2}. \end{aligned} \quad (\text{S1.7b})$$

Note that the quantum Langevin noise of zero mean satisfies  $\langle f_s(z) f_s^\dagger(z') \rangle = 2\gamma \delta(z - z')$  and  $\langle f_s^\dagger(z) f_s(z') \rangle = 0$ . The quantumness of quadrature PT symmetry can be further approached by analyzing the variances (or noise fluctuations) of  $q_j$  and  $p_j$  for the vacuum input state. After some algebra, we have reached the following important results:

$$\langle \Delta q_{i,0}^2 \rangle = \langle q_i^2(0) \rangle - \langle q_i(0) \rangle^2 = \frac{h(L) - 2\sin^2 \epsilon - \sec \epsilon \cos(2\beta L - \epsilon)}{8\cos^2(\beta L - \epsilon)}, \quad (\text{S1.8a})$$

$$\begin{aligned} \langle \Delta p_{s,L}^2 \rangle &= \langle p_s^2(L) \rangle - \langle p_s(L) \rangle^2 \\ &= \frac{h(L) \cos \epsilon - \cos(2\beta L + \epsilon) - 2\sin^2 \epsilon \cos(2\beta L - \epsilon)}{8 \cos \epsilon \cos^2(\beta L - \epsilon)}, \end{aligned} \quad (\text{S1.8b})$$

$$\langle \Delta q_{s,L}^2 \rangle = \langle q_s^2(L) \rangle - \langle q_s(L) \rangle^2 = \frac{2 + \cos^2 \varphi e^{-2\gamma L} - \cos \varphi \cos(2\kappa L + \varphi)}{8 \cos^2(\kappa L)}, \quad (\text{S1.8c})$$

$$\langle \Delta p_{i,0}^2 \rangle = \langle p_i^2(0) \rangle - \langle p_i(0) \rangle^2 = \frac{(2 + \cos^2 \varphi) e^{2\gamma L} - \cos \varphi \cos(2\kappa L - \varphi)}{8 \cos^2(\kappa L)}. \quad (\text{S1.8d})$$

where  $h(L) = 3 + 2\gamma L$  and  $\varphi = \arctan\left(\frac{\gamma}{\kappa}\right)$ . We notice from Eqs. (S1.8a)—(S1.8d) that although

these variances contain linear terms, they do not affect the periodic characteristics of the noise fluctuations. As revealed in Fig. 2 in the main text, when taking  $2\kappa L$  as the dimensionless variable, we find that the oscillation period of the variances of the PT-quadrature pair  $(q_i, p_s)$  is approximately to be  $\frac{2\kappa\pi}{\beta}$  while the fluctuation period of the variances of the non-PT quadrature pair  $(p_i, q_s)$  simply assumes  $2\pi$  for the parameter space in the PT-phase intact region.

As emphasized in the main text, the ultimate novelty of our work is not just to find a system capable of the observation of genuine quantum optical PT symmetry under fair sampling measurement, but to unearth an extraordinary phenomenon that has never been discovered. That is, the PT-quadrature observable enables one to witness a compelling quantum-to-classical transition perfectly coinciding with the PT phase transition by varying the non-Hermitian parameter  $\gamma$ , and the transition boundary is physically defined by the EP curve. To the best of our knowledge, this is the first proposal on exploring the untrivial transition between two incompatible worlds, classical and quantum, with a well-defined physical boundary by measuring the same quantum observable. We are aware that there exists a parallel way in the literature that exploits some massive quantum systems such as cooled cavity optomechanical structures to probe the quantum-to-classical transition by constantly checking the decoherence of a quantum state when manipulating some system parameters. However, even if these proposals are viable in the lab, they have to face an inescapable conundrum, that is, in these systems it becomes extremely challenging to determine the exact transition boundary. In other words, observing the sharp transition would be exceedingly difficult and even impossible for these protocols. In contrast, these difficulties do not appear in our system. Moreover, our method aims to measure the expectation of a quantum observable while the existing protocols concentrate on studying the state of the system. This difference fundamentally distinguishes our work from all others. All in all, our work for the first time presents a new way to explore the quantum-to-classical transition by taking advantage of non-Hermiticity and symmetry.

Before ending this part of discussion, here we would like to add a couple of additional comments on the following important issues on quantum optical PT symmetry raised in the literature. One is in response to the quantum noncloning theorem. In fact, the amplification won't violate the quantum noncloning theorem at all in our proposal, because the PSA here only acts on the single-mode idler field. This also concurs with the well-established knowledge in the field of quantum optics, especially in quantum squeezing. The second question concerns the law of causality. Although the gain may lead to the fast-light or superluminal effect, since the quantum noise introduced by the transmission loss is inseparable from the actual signal of interest, the causality proves not to be a problem when considering PT symmetry at the quantum level (as we did here).

## II. Derivation of quantum sensing

For the quantum sensor application, we consider the generation of the idler-signal bosonic modes from a seeding two-photon coherent state  $|\psi_i\rangle = |\alpha_1, \alpha_2\rangle$ . If taking into account the thermal reservoir with an average thermal bosonic number  $n_{\text{th}}$ , the quantum Langevin noise in Eq. (S1.3b) obeys the following properties,  $\langle f_s(z)f_s^\dagger(z')\rangle = 2\gamma(n_{\text{th}} + 1)\delta(z - z')$  and  $\langle f_s^\dagger(z)f_s(z')\rangle = 2\gamma n_{\text{th}}\delta(z - z')$ . After an interaction length  $L$ , the mean values and variances of the quadrature measurements on  $q_j$  and  $p_j$  with respect to the final state  $|\psi_f\rangle$  of the system can be obtained by using Eqs. (S1.6a) and (S1.6b),

$$\langle q_i(0)\rangle = \frac{\cos \epsilon}{\cos(\beta L - \epsilon)} \langle q_i(L)\rangle - \frac{\sin(\beta L)}{\cos(\beta L - \epsilon)} \langle p_s(0)\rangle, \quad (\text{S2.1a})$$

$$\langle p_s(L)\rangle = \frac{-\sin(\beta L)}{\cos(\beta L - \epsilon)} \langle q_i(L)\rangle + \frac{\cos \epsilon}{\cos(\beta L - \epsilon)} \langle p_s(0)\rangle, \quad (\text{S2.1b})$$

$$\langle q_s(L)\rangle = -\frac{\sin(\kappa L)}{\cos(\kappa L)} \langle p_i(L)\rangle + \frac{e^{-\gamma L}}{\cos(\kappa L)} \langle q_s(0)\rangle, \quad (\text{S2.1c})$$

$$\langle p_i(0) \rangle = \frac{e^{\gamma L}}{\cos(\kappa L)} \langle p_i(L) \rangle - \frac{\sin(\kappa L)}{\cos(\kappa L)} \langle q_s(0) \rangle, \quad (\text{S2.1d})$$

and

$$\langle \Delta q_{i,0}^2 \rangle = \frac{3 + w[2\gamma L - \tan\epsilon \sin(2\beta L)] - \cos(2\beta L) - 2\sin^2\epsilon}{8\cos^2(\beta L - \epsilon)}, \quad (\text{S2.2a})$$

$$\langle \Delta p_{s,L}^2 \rangle = \frac{3 + w[2\gamma L + \tan\epsilon \sin(2\beta L - 2\epsilon)] - \cos(2\beta L) + 4n_{\text{th}}\sin^2\epsilon}{8\cos^2(\beta L - \epsilon)}, \quad (\text{S2.2b})$$

$$\begin{aligned} \langle \Delta q_{s,L}^2 \rangle \\ = \frac{w[\cos(2\kappa L) - \cos\varphi \cos(2\kappa L + \varphi) + 1] + [\cos^2\varphi - 2(1 + \sin^2\varphi)n_{\text{th}}]e^{-2\gamma L} + 2\sin^2(\kappa L)}{8\cos^2(\kappa L)}, \end{aligned} \quad (\text{S2.2c})$$

$$\begin{aligned} \langle \Delta p_{i,0}^2 \rangle \\ = \frac{w\{[\cos^2\varphi(e^{2\gamma L} - 1) - 2\sin^2\varphi] - 2\sin\varphi \cos(\kappa L) \sin(\kappa L - \varphi)\} + 2[e^{2\gamma L} + \sin^2(\kappa L)]}{8\cos^2(\kappa L)}. \end{aligned} \quad (\text{S2.2d})$$

Here,  $w = 2n_{\text{th}} + 1$  with the thermal average boson number  $n_{\text{th}} = \left[ \text{Exp}\left(\frac{h\nu_\lambda}{k_B T}\right) - 1 \right]^{-1}$ . One can easily check that the thermal photon number becomes infinitesimal at the room temperature ( $\sim 300$  K) in the visible spectral range. Alternatively, the above Langevin noise properties reduce to the simpler formats mentioned in Section I.

The ultimate precision of the parameter estimation of  $\kappa$  is essentially determined by the variance  $\Delta_\kappa^2$  in terms of a targeted physical observable. The performance of the proposed quadrature-PT sensing scheme can be however evaluated by comparing the inverse variances  $\Delta_{\kappa,q_j}^{-2} = \frac{(\chi_\kappa^{q_j})^2}{\langle \Delta q_j^2 \rangle}$  and  $\Delta_{\kappa,p_j}^{-2} = \frac{(\chi_\kappa^{p_j})^2}{\langle \Delta p_j^2 \rangle}$  with the quantum Fisher information  $F_\kappa$  at the system's final state  $|\psi_f\rangle$ . Here, we have introduced the susceptibilities  $\chi_\kappa^{q_j} = \partial_\kappa \langle q_j \rangle$  and  $\chi_\kappa^{p_j} = \partial_\kappa \langle p_j \rangle$  to capture the system response to  $\langle q_j \rangle$  and  $\langle p_j \rangle$  for a small perturbation  $\delta\kappa$  about the preset  $\kappa$ . With the help of Eqs. (S2.1a)—(S2.1d), after some labor one can show that  $\chi_\kappa^{q_j}$  and  $\chi_\kappa^{p_j}$  ( $j = i, s$ ) take the form of,

$$\chi_\kappa^{q_{i(0)}} = \frac{\alpha\{2\beta L[\sin(\beta L) - 1] + \sin\epsilon [2\sin(\beta L) + \cos(\beta L - \epsilon) - \cos\epsilon]\}}{2\beta\cos^2(\beta L - \epsilon)}, \quad (\text{S2.3a})$$

$$\chi_\kappa^{p_{s(L)}} = \chi_\kappa^{q_{i(0)}}, \quad (\text{S2.3b})$$

$$\chi_\kappa^{q_{s(L)}} = \alpha L \sec^2(\kappa L)[e^{-\gamma L} \sin(\kappa L) - 1], \quad (\text{S2.3c})$$

$$\chi_\kappa^{p_{i(0)}} = \alpha L \sec^2(\kappa L)[e^{\gamma L} \sin(\kappa L) - 1]. \quad (\text{S2.3d})$$

By plugging Eqs. (S2.2a)—(S2.2d) and Eqs. (S2.3a)—(S2.3d) into the inverse variances  $\Delta_{\kappa,q_j}^{-2} = \frac{(\chi_\kappa^{q_j})^2}{\langle \Delta q_j^2 \rangle}$

and  $\Delta_{\kappa,p_j}^{-2} = \frac{(\chi_\kappa^{p_j})^2}{\langle \Delta p_j^2 \rangle}$ , we arrive at the following key results:

$$\langle \Delta_{\kappa,q_{i,0}}^{-2} \rangle = \frac{2\alpha^2\{2\beta L[\sin(\beta L) - 1] + \sin\epsilon [2\sin(\beta L) + \cos(\beta L - \epsilon) - \cos\epsilon]\}^2}{\beta^2\cos^2(\beta L - \epsilon)\{3 + w[2\gamma L - \tan\epsilon \sin(2\beta L)] - \cos(2\beta L) - 2\sin^2\epsilon\}}, \quad (\text{S2.4a})$$

$$\langle \Delta_{\kappa,p_{s,L}}^{-2} \rangle = \frac{2\alpha^2\{2\beta L[\sin(\beta L) - 1] + \sin\epsilon [2\sin(\beta L) + \cos(\beta L - \epsilon) - \cos\epsilon]\}^2}{\beta^2\cos^2(\beta L - \epsilon)\{3 + w[2\gamma L + \tan\epsilon \sin(2\beta L - 2\epsilon)] - \cos(2\beta L) + 4n_{\text{th}}\sin^2\epsilon\}}, \quad (\text{S2.4b})$$

$$\begin{aligned} \langle \Delta_{\kappa,q_{s,L}}^{-2} \rangle \\ = \frac{8\alpha^2 L^2 \sec^2(\kappa L)[e^{-\gamma L} \sin(\kappa L) - 1]^2}{w[\cos(2\kappa L) - \cos\varphi \cos(2\kappa L + \varphi) + 1] + [\cos^2\varphi - 2(1 + \sin^2\varphi)n_{\text{th}}]e^{-2\gamma L} + 2\sin^2(\kappa L)}, \end{aligned} \quad (\text{S2.4c})$$

$$\begin{aligned} & \langle \Delta_{\kappa, p_{i,0}}^{-2} \rangle \\ &= \frac{8\alpha^2 L^2 \sec^2(\kappa L) [e^{\gamma L} \sin(\kappa L) - 1]^2}{w\{\cos^2\varphi(e^{2\gamma L} - 1) - 2\sin^2\varphi\} - 2\sin\varphi \cos(\kappa L) \sin(\kappa L - \varphi) + 2[e^{2\gamma L} + \sin^2(\kappa L)]}. \end{aligned} \quad (\text{S2.4d})$$

After having the inverse variances (S2.4a)—(S2.4d), now let us turn our attention to the quantum Fisher information  $F_\kappa$ , i.e., the quantum Cramér-Rao bound, which demands the optimal measurement to satisfy the inequality  $\Delta_\kappa^{-2} \leq F_\kappa$ . In this sensing protocol, we start with the initial system state to be in a two-photon coherent state  $|\psi_i\rangle = |\alpha_1, \alpha_2\rangle$  for the sake of simplicity. Then, the final state of the system evolves as  $|\psi_f\rangle = \frac{U}{\sqrt{\mu}}|\psi_i\rangle$ , where  $U = e^{-iHL}$  is the evolution operator and  $\mu = \langle \psi_f | \psi_f \rangle$  is the normalization coefficient. By working in the Schrödinger picture and treating the idler-signal field operators  $a_i = a_i(L)$  and  $a_s = a_s(0)$  as constant operators, the quantum Fisher information can be calculated by the definition of  $F_\kappa = 4 \left( \langle \partial_\kappa \psi_f | \partial_\kappa \psi_f \rangle - |\langle \partial_\kappa \psi_f | \psi_f \rangle|^2 \right)$  for a parameter  $\kappa$  that controls the strength of the system's Hamiltonian  $H$  (S1.1) with respect to a known physical observable (in our case, it can be any of the four quadratures). To this end, let us give a detailed examination on the first term in  $F_\kappa$ :

$$\begin{aligned} & \langle \partial_\kappa \psi_f | \partial_\kappa \psi_f \rangle \\ &= \langle \psi_i | \frac{\sqrt{\mu}(\partial_\kappa U^\dagger) - \frac{\partial_\kappa \mu}{2\sqrt{\mu}} U^\dagger}{\mu} \frac{\sqrt{\mu}(\partial_\kappa U) - \frac{\partial_\kappa \mu}{2\sqrt{\mu}} U}{\mu} | \psi_i \rangle \\ &= L^2 \langle \psi_f | \partial_\kappa H^\dagger \partial_\kappa H | \psi_f \rangle - iL \frac{\partial_\kappa \mu}{2\sqrt{\mu}} \langle \psi_f | \partial_\kappa H^\dagger | \psi_f \rangle + iL \frac{\partial_\kappa \mu}{2\sqrt{\mu}} \langle \psi_f | \partial_\kappa H | \psi_f \rangle + \frac{(\partial_\kappa \mu)^2}{4\mu^2}, \end{aligned} \quad (\text{S2.5})$$

where  $\partial_\kappa U = -iL(\partial_\kappa H)U$ . Note that  $\partial_\kappa H$  commutes with  $U$ . In the same way, we can also obtain the exact expression for the second term as follows:

$$\begin{aligned} & |\langle \partial_\kappa \psi_f | \psi_f \rangle|^2 \\ &= L^2 \langle \psi_f | \partial_\kappa H^\dagger | \psi_f \rangle \langle \psi_f | \partial_\kappa H | \psi_f \rangle - iL \frac{\partial_\kappa \mu}{2\sqrt{\mu}} \langle \psi_f | \partial_\kappa H^\dagger | \psi_f \rangle + iL \frac{\partial_\kappa \mu}{2\sqrt{\mu}} \langle \psi_f | \partial_\kappa H | \psi_f \rangle + \frac{(\partial_\kappa \mu)^2}{4\mu^2}. \end{aligned} \quad (\text{S2.6})$$

Substituting these two results into  $F_\kappa$  yields the concise and intuitive expression of the quantum Fisher information, which is

$$F_\kappa = 4L^2 \left( \langle \psi_f | \partial_\kappa H^\dagger \partial_\kappa H | \psi_f \rangle - \langle \psi_f | \partial_\kappa H^\dagger | \psi_f \rangle \langle \psi_f | \partial_\kappa H | \psi_f \rangle \right). \quad (\text{S2.7})$$

Since  $\partial_\kappa H = \partial_\kappa H^\dagger = \hbar(a_i^\dagger a_s^\dagger + a_i a_s) = 2\hbar(q_i q_s - p_s p_i)$  in the Schrödinger picture and the expectation value of an operator does not change along with the picture transformation, we can transform the above formulae of the quantum Fisher information into the Heisenberg representation to ease the calculations. That is,

$$\begin{aligned} F_\kappa &= 16L^2 \left( \langle \psi_f | (q_i q_s - p_s p_i)^2 | \psi_f \rangle - (\langle \psi_f | q_i q_s - p_s p_i | \psi_f \rangle)^2 \right) \\ &= 16L^2 \{ \langle \psi_i | [q_i(0)q_s(L) - p_s(L)p_i(0)]^2 | \psi_i \rangle \\ &\quad - [\langle \psi_i | [q_i(0)q_s(L) - p_s(L)p_i(0)] | \psi_i \rangle]^2 \} \\ &= 16L^2 \{ ([q_i(0)q_s(L) - p_s(L)p_i(0)]^2 - \langle q_i(0)q_s(L) - p_s(L)p_i(0) \rangle^2) \}. \end{aligned} \quad (\text{S2.8})$$

From Eq. (S2.8), one can easily evaluate the term  $q_i(0)q_s(L) - p_s(L)p_i(0)$  using Eqs. (S1.6a) and (S1.6b). After some lengthy derivations, we eventually get

$$\begin{aligned} & q_i(0)q_s(L) - p_s(L)p_i(0) \\ &= Aq_i(L)p_i(L) + Bp_s(0)p_i(L) + \int_0^L dz C P_s p_i(L) + Dq_i(L)q_s(0) \\ &+ Ep_s(0)q_s(0) + \int_0^L dz F P_s q_s(0) + \int_0^L dz G Q_s q_i(L) + \int_0^L dz J Q_s p_s(0) \\ &+ \int_0^L dz R P_s Q_s, \end{aligned} \quad (\text{S2.9})$$

where all the involved coefficients are

$$A = \frac{e^{\gamma L} \sin(\beta L) - \cos \epsilon \sin(\kappa L)}{\cos(\beta L - \epsilon) \cos(\kappa L)}, \quad (\text{S2.10a})$$

$$B = \frac{\sin(\beta L) \sin(\kappa L) - e^{\gamma L} \cos \epsilon}{\cos(\beta L - \epsilon) \cos(\kappa L)}, \quad (\text{S2.10b})$$

$$C = \frac{\sin[\beta(L-z)] \sin(\kappa L) - e^{\gamma L} \cos(\beta z - \epsilon)}{\cos(\beta L - \epsilon) \cos(\kappa L)}, \quad (\text{S2.10c})$$

$$D = \frac{e^{-\gamma L} \cos \epsilon - \sin(\beta L) \sin(\kappa L)}{\cos(\beta L - \epsilon) \cos(\kappa L)}, \quad (\text{S2.10d})$$

$$E = \frac{\cos \epsilon \sin(\kappa L) - e^{-\gamma L} \sin(\beta L)}{\cos(\beta L - \epsilon) \cos(\kappa L)}, \quad (\text{S2.10e})$$

$$F = \frac{\sin(\kappa L) \cos(\beta z - \epsilon) - e^{-\gamma L} \sin(\beta(L-z))}{\cos(\beta L - \epsilon) \cos(\kappa L)}, \quad (\text{S2.10f})$$

$$G = \frac{e^{\gamma(z-L)} \cos(\kappa z) \cos \epsilon - e^{\gamma z} \sin[\kappa(L-z)] \sin(\beta L)}{\cos(\beta L - \epsilon) \cos(\kappa L)}, \quad (\text{S2.10g})$$

$$J = \frac{e^{\gamma z} \sin[\kappa(L-z)] \cos \epsilon - e^{\gamma(z-L)} \cos(\kappa z) \sin(\beta L)}{\cos(\beta L - \epsilon) \cos(\kappa L)}, \quad (\text{S2.10h})$$

$$R = \frac{e^{\gamma z} \sin[\kappa(L-z)] \cos(\beta z - \epsilon) - e^{\gamma(z-L)} \cos(\kappa z) \sin[\beta(L-z)]}{\cos(\beta L - \epsilon) \cos(\kappa L)}. \quad (\text{S2.10i})$$

With these results, we are ready to work out the following step,

$$\begin{aligned} & \langle [q_i(0)q_s(L) - p_s(L)p_i(0)]^2 \rangle - \langle q_i(0)q_s(L) - p_s(L)p_i(0) \rangle^2 \\ &= A^2 (\langle q_i(L)p_i(L)q_i(L)p_i(L) \rangle - \langle q_i(L)p_i(L) \rangle^2) \\ &+ B^2 (\langle p_i^2(L)p_s^2(0) \rangle - \langle p_s(0)p_i(L) \rangle^2) + D^2 (\langle q_i^2(L)q_s^2(0) \rangle - \langle q_s(0)q_i(L) \rangle^2) \\ &+ E^2 (\langle p_s(0)q_s(0)p_s(0)q_s(0) \rangle - \langle p_s(0)q_s(0) \rangle^2) \\ &+ AB (\langle p_i(L)q_i(L)p_i(L) \rangle + \langle q_i(L)p_i(L)p_i(L) \rangle \\ &- 2\langle p_i(L) \rangle \langle q_i(L)p_i(L) \rangle) \langle p_s(0) \rangle \\ &+ AD (\langle q_i(L)q_i(L)p_i(L) \rangle + \langle q_i(L)p_i(L)q_i(L) \rangle \\ &- 2\langle q_i(L) \rangle \langle q_i(L)p_i(L) \rangle) \langle q_s(0) \rangle \\ &+ BE (\langle p_s(0)q_s(0)p_s(0) \rangle + \langle p_s(0)p_s(0)q_s(0) \rangle \\ &- 2\langle p_s(0) \rangle \langle p_s(0)q_s(0) \rangle) \langle p_i(L) \rangle \\ &+ DE (\langle p_s(0)q_s(0)q_s(0) \rangle + \langle q_s(0)p_s(0)q_s(0) \rangle \\ &- 2\langle q_s(0) \rangle \langle p_s(0)q_s(0) \rangle) \langle q_i(L) \rangle \\ &+ BD (\langle q_i(L)p_i(L)q_s(0)p_s(0) \rangle + \langle p_i(L)q_i(L)p_s(0)q_s(0) \rangle \\ &- 2\langle q_i(L) \rangle \langle q_s(0) \rangle \langle p_i(L) \rangle \langle p_s(0) \rangle) \\ &+ \int_0^L dz [C^2 \langle p_i^2(L) \rangle + F^2 \langle q_s^2(0) \rangle + 2CF \langle q_s(0)p_i(L) \rangle] \langle P_s^2 \rangle \\ &+ \int_0^L dz [G^2 \langle q_i^2(L) \rangle + J^2 \langle p_s^2(0) \rangle + 2GJ \langle p_s(0)q_i(L) \rangle] \langle Q_s^2 \rangle \\ &+ \int_0^L dz CG [\langle q_i(L)p_i(L) \rangle \langle Q_s P_s \rangle + \langle p_i(L)q_i(L) \rangle \langle P_s Q_s \rangle] \\ &+ \int_0^L dz FJ [\langle p_s(0)q_s(0) \rangle \langle Q_s P_s \rangle + \langle q_s(0)p_s(0) \rangle \langle P_s Q_s \rangle] + \int_0^L dz R^2 \langle P_s Q_s P_s Q_s \rangle \\ &- \left( \int_0^L dz R \langle P_s Q_s \rangle \right)^2, \end{aligned} \quad (\text{S2.11})$$

in terms of the quadrature operators at the initial boundary conditions. By further simplification, we finally approach the following resultant function for the quantum Fisher information,

$$F_\kappa = 16L^2 \left[ (A^2 + E^2) \left( \frac{\alpha^2}{2} + \frac{1}{8} \right) + (AB + AD + BE + DE) \left( \frac{\alpha^2}{2} \right) + \left( \frac{1}{16} + \frac{\alpha^2}{2} \right) (B^2 + D^2) - \frac{1}{8} BD + \left( \frac{1}{4} + \alpha^2 \right) \frac{\gamma}{2} (2n_{\text{th}} + 1) \int_0^L dz (C^2 + F^2 + G^2 + J^2) + \alpha^2 \gamma (2n_{\text{th}} + 1) \int_0^L dz (CF + JG) + \frac{\gamma}{4} \int_0^L dz (JF - CG) + \frac{\gamma}{2} \left( n_{\text{th}} + \frac{\gamma}{2} \right) \int_0^L dz R^2 + \frac{\gamma^2}{4} \left( \int_0^L dz R \right)^2 \right]. \quad (\text{S2.12})$$

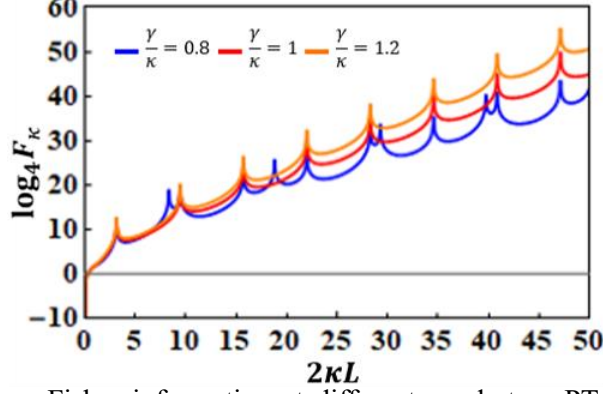


FIG. S1. The quantum Fisher information at different quadrature PT states. Blue, red, and orange lines are, respectively, corresponding to  $\gamma/\kappa = 0.8$  (unbroken quadrature-PT phase),  $\gamma/\kappa = 1$  (EP point), and  $\gamma/\kappa = 1.2$  (broken quadrature-PT phase).

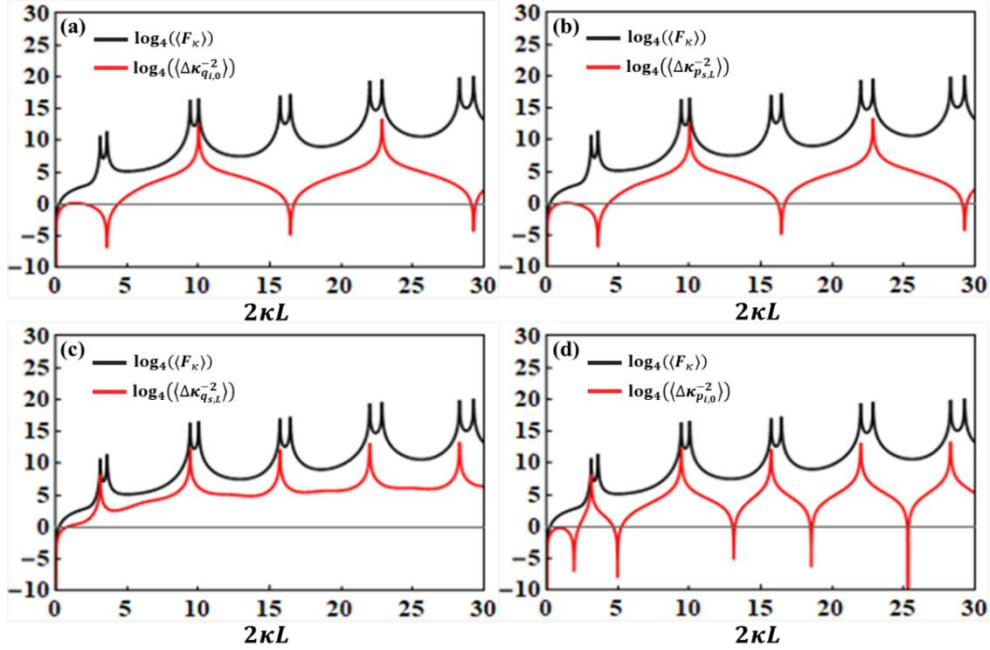


FIG. S2. Quantum sensing performance by comparing  $\log_4(\Delta\kappa_{q_{i,0}}^{-2})$  (a),  $\log_4(\Delta\kappa_{p_{s,L}}^{-2})$  (b),  $\log_4(\Delta\kappa_{q_{s,L}}^{-2})$  (c), and  $\log_4(\Delta\kappa_{p_{i,0}}^{-2})$  (d) with  $\log_4 F_\kappa$  in the quadrature-PT phase unbroken region for the parameters ( $\alpha = 2$ ,  $\gamma = 0.2$ ,  $\kappa = 1$ ).

Obviously, the quantum Fisher information  $F_\kappa$  (S2.12) will feature different manifestations in response to the contrasting PT domains of the system. As a representative example, in Fig. S1 we accordingly present the quantum Fisher information  $\log_4 F_\kappa$  for three distinct scenarios:  $\frac{\gamma}{\kappa} = 0.8$  (unbroken quadrature-PT phase),  $\frac{\gamma}{\kappa} = 1$  (EP point), and  $\frac{\gamma}{\kappa} = 1.2$  (breaking quadrature-PT phase).

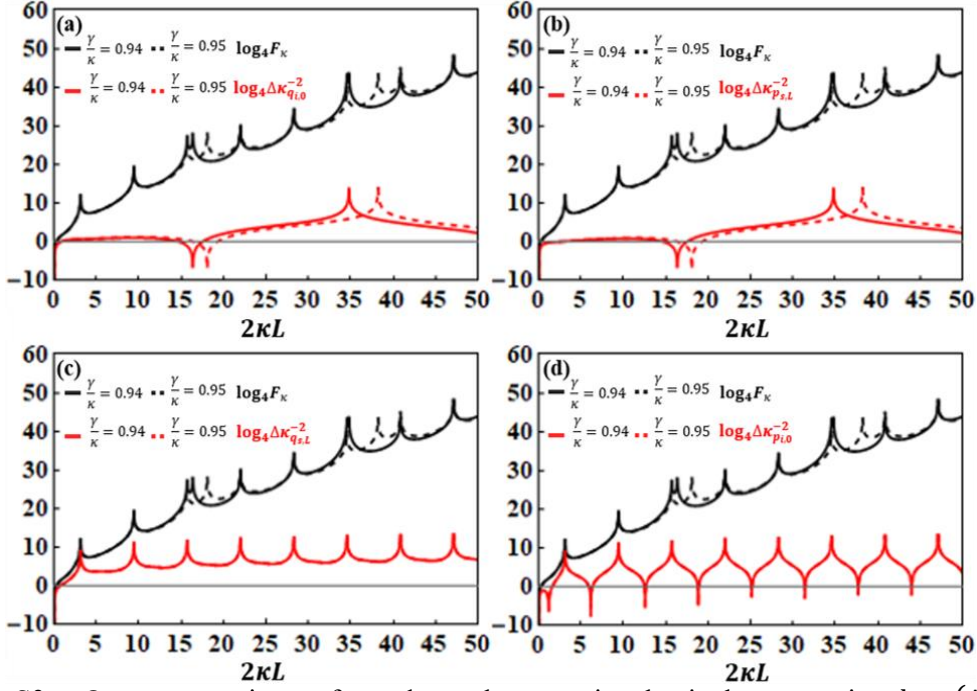


FIG. S3. Quantum sensing performed near the exceptional point by comparing  $\log_4(\Delta \kappa_{q_{i,0}}^{-2})$  (a),  $\log_4(\Delta \kappa_{p_{s,L}}^{-2})$  (b),  $\log_4(\Delta \kappa_{q_{s,L}}^{-2})$  (c), and  $\log_4(\Delta \kappa_{p_{i,0}}^{-2})$  (d) with  $\log_4 F_k$  for  $\frac{\gamma}{\kappa} = 0.94$  and  $\frac{\gamma}{\kappa} = 0.95$  for the parameters  $\alpha = 2$  and  $\kappa = 1$ .

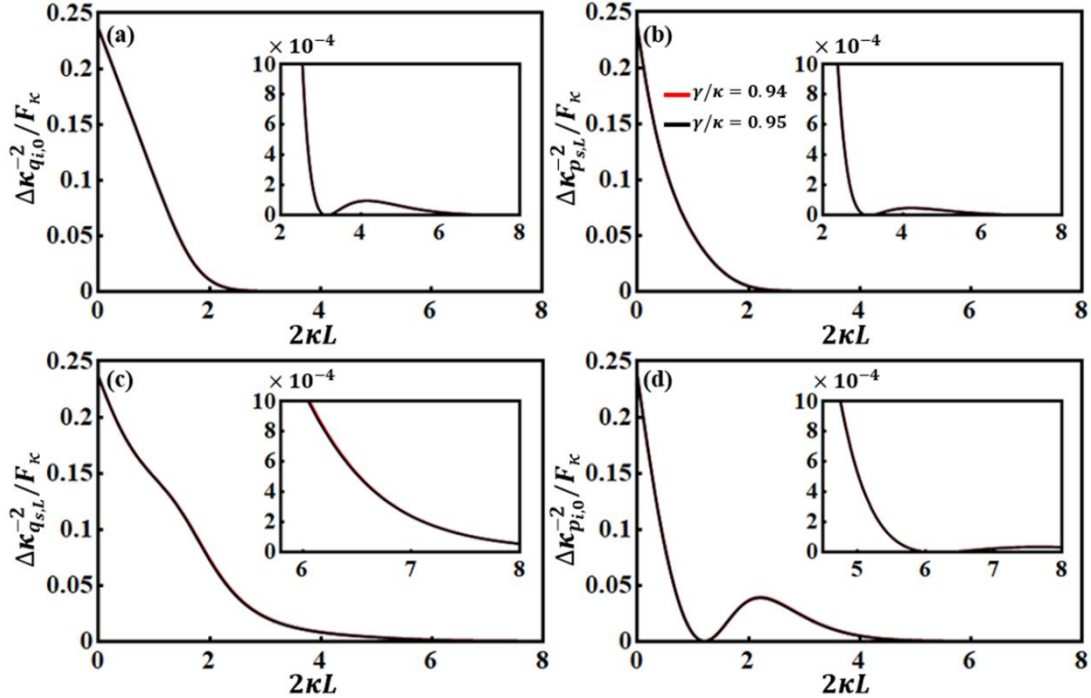


FIG. S4. Evaluating quantum sensing performance (FIGs. S3(a)—(d)) near the exceptional point by examining the ratios of  $\Delta \kappa_{q_{i,0}}^{-2}$  (a),  $\Delta \kappa_{p_{s,L}}^{-2}$  (b),  $\Delta \kappa_{q_{s,L}}^{-2}$  (c), and  $\Delta \kappa_{p_{i,0}}^{-2}$  (d) to  $F_k$  for  $\frac{\gamma}{\kappa} = 0.94$  (red curve) and  $\frac{\gamma}{\kappa} = 0.95$  (black curve), respectively. The other parameters are  $\alpha = 2$  and  $\kappa = 1$ .

Different from other existing (quantum) sensing protocols based on PT or EP enhancement, we find that the PT-quadrature variables permit optimal classical sensor performance in the PT phase unbroken regime but far away from the EP. This observation is strongly supported by analyzing the quantum Fisher information with respect to the inverse variances across the parameter space. In the main text,

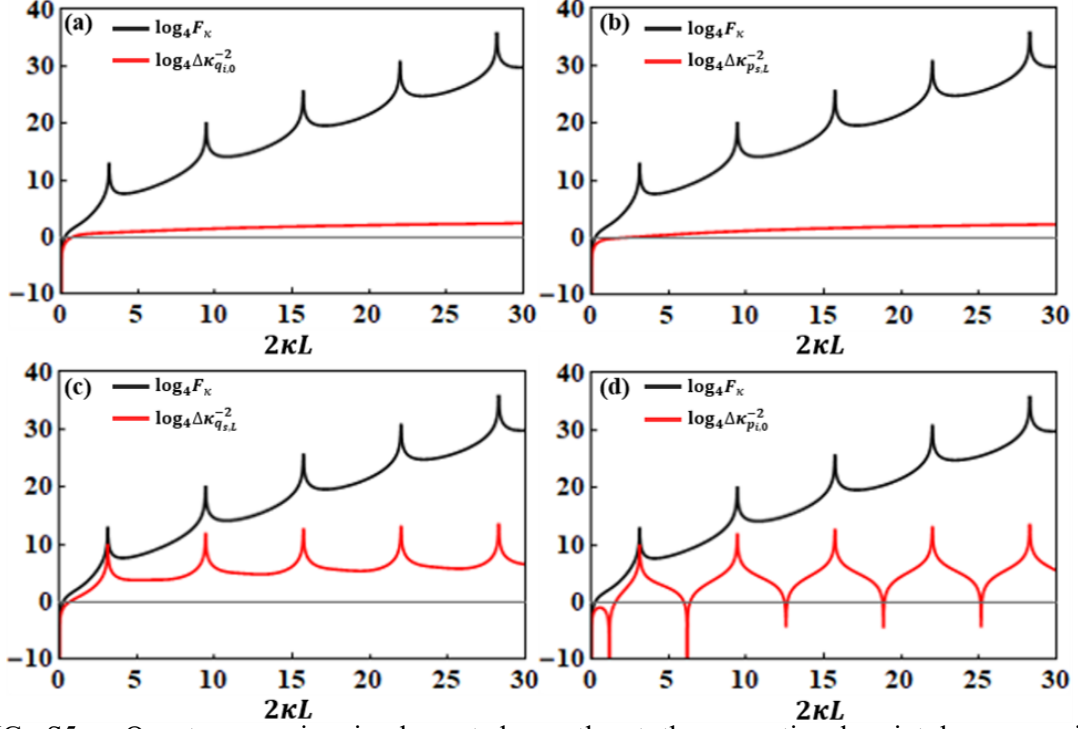


FIG. S5. Quantum sensing implemented exactly at the exceptional point by comparing  $\log_4(\Delta\kappa_{q_{i,0}}^{-2})$  (a),  $\log_4(\Delta\kappa_{p_{s,L}}^{-2})$  (b),  $\log_4(\Delta\kappa_{q_{s,L}}^{-2})$  (c), and  $\log_4(\Delta\kappa_{p_{i,0}}^{-2})$  (d) with  $\log_4 F_\kappa$  for  $\alpha = 2$  and  $\kappa = 1$ .

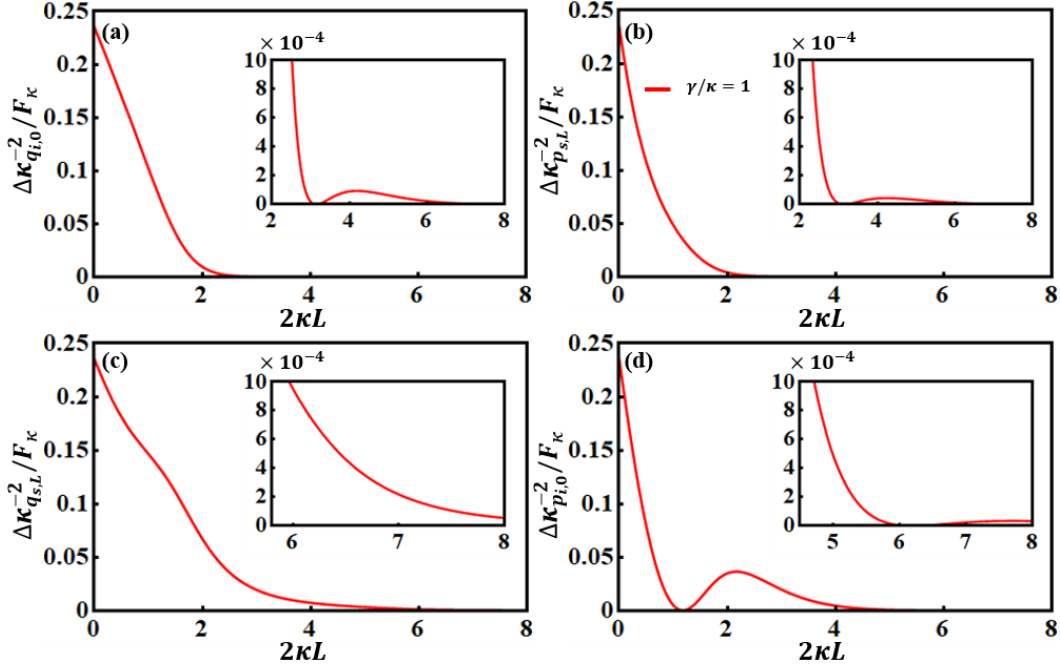


FIG. S6. Evaluating quantum sensing performance (FIG. S5(a)–(d)) at the exceptional point by examining the ratios of  $\Delta\kappa_{q_{i,0}}^{-2}$  (a),  $\Delta\kappa_{p_{s,L}}^{-2}$  (b),  $\Delta\kappa_{q_{s,L}}^{-2}$  (c), and  $\Delta\kappa_{p_{i,0}}^{-2}$  (d) to  $F_\kappa$  for the parameters  $\alpha = 2$  and  $\kappa = 1$ .

we have shown the precision of the  $\kappa$ -parameter estimation by looking at the ratio of the inverse variance  $\Delta\kappa^{-2}$  to the quantum Fisher information  $F_\kappa$  in Figs. 5(a)–(d), which should be bounded in the range of  $[0, 1]$ . In Fig. S2(a)–(d), we have further given these inverse variances in comparison with  $F_\kappa$ . To make the point more straightforward and convincing, in Figs. S3(a)–(d) we have particularly examined the measurement schemes implemented very close to the EP for  $\frac{\gamma}{\kappa} = 0.94$  and

$\frac{\gamma}{\kappa} = 0.95$  by plotting  $\log_4 \Delta\kappa_{q_{i,0}}^{-2}$ ,  $\log_4 \Delta\kappa_{p_{s,L}}^{-2}$ ,  $\log_4 \Delta\kappa_{q_{s,L}}^{-2}$ , and  $\log_4 \Delta\kappa_{p_{i,0}}^{-2}$ . Similarly, the quantitative sensing performance offered by each quadrature can be well assessed by evaluating the corresponding ratio of  $\Delta\kappa_{q_{i,0}}^{-2}$  (Fig. S4(a)),  $\Delta\kappa_{p_{s,L}}^{-2}$  (Fig. S4(b)),  $\Delta\kappa_{q_{s,L}}^{-2}$  (Fig. S4(c)), and  $\Delta\kappa_{p_{i,0}}^{-2}$  (Fig. S4(d)) to  $F_\kappa$  for the same parameters used in Figs. S3(a)—(d). By comparing these figures with Figs. 5(a)—(d) in the main text, it is not difficult to conclude that indeed, the presence of gain and loss in gain-loss-coupled PT symmetry can substantially diminish the EP-based super-sensitivity promised in the classical settings and make it unavailable in the quantum level. Moreover, even if one still insists on performing any quantum sensing measurement in the vicinity of the EP (e.g.,  $\frac{\gamma}{\kappa} = 0.94$  and  $\frac{\gamma}{\kappa} = 0.95$ ), it would become highly challenging due to the vast difference between the peak values of  $\Delta\kappa^{-2}$  and  $F_\kappa$  spanning over many orders of magnitude, regardless of whether the quadrature observables are associated with the characteristics of PT symmetry. This is especially true if comparing with the measurement carried out at  $\frac{\gamma}{\kappa} = 0.2$ .

What happens if one attempts to fulfill the quantum sensing at the phase transition point? In such a case, unfortunately, the paired PT quadratures will cease to showcase any response to the parameter precision estimation, thereby making them fully unsuitable for quantum sensor applications when the symmetry spontaneously breaks down. As demonstrated in Figs. S5(a) and (b), one can clearly see that  $\log_4 \Delta\kappa_{q_{i,0}}^{-2}$  and  $\log_4 \Delta\kappa_{p_{s,L}}^{-2}$  for the PT-symmetric quadrature pair  $(q_i(0), p_s(L))$  become smooth and curvatureless, indicating that they are completely insensitive to any perturbation on an unknown parameter yet to be estimated. Alternatively, no gain on parameter estimation will be accessed at the EP. On the other hand, we notice from Figs. S5(c) and (d) that the non-PT-symmetric quadrature pair  $(p_i(0), q_s(L))$  enables best sensing measurement only near the first peaks of the inverse variances  $\log_4 \Delta\kappa_{q_{s,L}}^{-2}$ , and  $\log_4 \Delta\kappa_{p_{i,0}}^{-2}$ , in accordance with the quantum Fisher information  $\log_4 F_\kappa$ . Obviously, this behaves differently from the cases of  $\frac{\gamma}{\kappa} = 0.2$ , where the supersensitive measurements are available near the first two peaks of  $\Delta\kappa^{-2}$  and even more peaks (Figs. S2(c) and (d)). In fact, when PT symmetry disappears, the quadrature pair  $(q_i(0), p_s(L))$  lose to offer any sensing capabilities, despite (sub)optimal sensing may be accessible to the other non-PT-symmetric conjugate pair  $(p_i(0), q_s(L))$ , according to our numerical simulations. To have a more intuitive evaluation on the quantum sensing performance exactly at the EP, it is better to look at the ratios of  $\Delta\kappa_{q_{i,0}}^{-2}$  (Fig. S6(a)),  $\Delta\kappa_{p_{s,L}}^{-2}$  (Fig. S6(b)),  $\Delta\kappa_{q_{s,L}}^{-2}$  (Fig. S6(c)), and  $\Delta\kappa_{p_{i,0}}^{-2}$  (Fig. S6(d)) to  $F_\kappa$  in the same way as we did above. From Figs. S6(a)—(d), we can easily find that these ratios quickly approach zero for the longer medium length  $L$ , implying that the system loses its sensing ability at the EP.

## References:

- [1] Jiang, Y., Mei, Y., Zuo, Y., Zhai, Y., Li, J., Wen, J. & Du, S. Anti-parity-time symmetry optical four-wave mixing in cold atoms. *Phys. Rev. Lett.* **123**, 193604 (2019).
- [2] Wang, W., Zhai, Y., Liu, D., Jiang, X., Ghamsari, S. V. & Wen, J. Quadrature parity-time symmetry. (2022)